"Effect of High Frequency Pulsing on the Interfacial Structure of Anodized Aluminium-TiO2"

Gudla, Visweswara Chakravarthy ; Jensen, Flemming ; Bordo, Kirill ; Simar, Aude ; Ambat, Rajan

Abstract

High frequency anodizing of friction stir processed Al-TiO2 surface composites was investigated. The effect of anodizing parameters on the structure and morphology of the anodic layer including the incorporation of the TiO2 particles into the anodic layer is studied. Anodizing process was carried out using a high frequency pulse and pulse reverse pulse technique at a fixed frequency in a sulfuric acid bath. The structure of the composites and the anodized layer was studied using scanning and transmission electron microscopy. The pulse reverse pulse anodizing technique, using a negative potential on the low voltage cycle, showed extensive pore branching and pore generation at the TiO2 particle-anodic alumina matrix interface. However, the pulse anodizing technique using zero potential during the low voltage cycle showed no such features in the pore morphology, but only entrapment of TiO2 particles into the anodic alumina. Lower electrical resistance of the TiO2 arising from oxygen def...

Document type : *Article de périodique (Journal article)*

Journal of The Electrochemical Society, **162** (7) C303-C310 (2015)
0013-4651/2015/162(7)/C303/8/$33.00 © The Electrochemical Society

Effect of High Frequency Pulsing on the Interfacial Structure of Anodized Aluminium-TiO_2

Visweswara Chakravarthy Gudla,[a,z] Flemming Jensen,[a,b] Kirill Bordo,[a] Aude Simar,[c] and Rajan Ambat[a]

[a]*Department of Mechanical Engineering, Technical University of Denmark, Produktionstorvet, DK-2800 Kgs. Lyngby, Denmark*
[b]*Bang & Olufsen A/S, Peter Bangs Vej 15, DK-7600 Struer, Denmark*
[c]*iMMC, Université Catholique de Louvain, 1348 Louvain-la-Neuve, Belgium*

High frequency anodizing of friction stir processed Al-TiO_2 surface composites was investigated. The effect of anodizing parameters on the structure and morphology of the anodic layer including the incorporation of the TiO_2 particles into the anodic layer is studied. Anodizing process was carried out using a high frequency pulse and pulse reverse pulse technique at a fixed frequency in a sulfuric acid bath. The structure of the composites and the anodized layer was studied using scanning and transmission electron microscopy. The pulse reverse pulse anodizing technique, using a negative potential on the low voltage cycle, showed extensive pore branching and pore generation at the TiO_2 particle-anodic alumina matrix interface. However, the pulse anodizing technique using zero potential during the low voltage cycle showed no such features in the pore morphology, but only entrapment of TiO_2 particles into the anodic alumina. Lower electrical resistance of the TiO_2 arising from oxygen defects, combined with applied negative potential during the low voltage cycle, are found to be responsible for the observed morphological features in the anodic alumina.

Manuscript submitted February 20, 2015; revised manuscript received March 23, 2015. Published March 31, 2015.

Anodizing is a widely applied surface finishing technique for Al and its alloys that are used in automobile, architecture, and aerospace industry. Anodized Al surfaces provide improved corrosion and wear resistance and more importantly pleasing aesthetics.[1,2] Different optical appearances for decorative purposes by coloring of the anodized layer are produced by pore filling using organic or inorganic dyes.[3–5] Recently, attempts have been made for less intense optical shades using magnetron sputtered binary coatings of specific compositions[6–8] and anodizing of Al based metal matrix composites like Al-TiO_2.[9] Varying levels of bright and white anodized appearance was generated with the help of light scattering from the incorporated TiO_2 in an otherwise transparent anodic alumina matrix. However, the anodic layer obtained for magnetron sputtered coatings as well as for Al-TiO_2 composites under conventional DC anodizing conditions was non-uniform in terms of completeness of the oxidation of different phases and the morphology of the anodic structure. These non-uniformities are attributed to the inherent electrochemical heterogeneity of the multiphase surfaces being anodized, which leads to an anodized layer with un-anodized or partially anodized Al based second phases as reported for commercial aluminum alloys.[10–12] In the case of Al-TiO_2 composites, the morphology of TiO_2 was altered, while electrochemical shadowing of the underlying Al by TiO_2 caused the presence of un-anodized Al beneath the particles.[9] Overall the presence of heterogeneities in the metallic form in the anodized layer cause darkening and dull appearance of the anodized layer.[13–16]

The Al-Si cast alloys, due to their heterogeneity and passivating nature of primary Si phase, pose similar challenges during conventional DC anodizing. Ono et al.[17] used a high frequency electrolysis technique to investigate the effect on uniformity of the anodized surface of a cast Al-Si (AC8A) alloy. It has been found that the high frequency pulsing provides effective anodizing of Al even below the incorporated primary Si phase due to pore branching, which otherwise is shadowed in conventional DC anodizing. Kanagaraj et al.[18,19] studied the effect of pulse frequency and duty cycle on the anodizing of AA1100 and reported that better quality anodic films are obtained at higher frequencies when compared to lower frequencies.

Juhl et al.[20] have pulse anodized Al alloys (both extruded and cast) and investigated different pulsing techniques namely: (i) low frequency pulsing,[21] (ii) high frequency pulsing,[22] and (iii) pulse reverse pulsing technique.[23,24] The hardness of the anodic layers was found to be lower for the pulse reverse pulse anodized surfaces when compared to the other two techniques. However, the structure of the anodic layers obtained did not show considerable differences as observed using scanning electron microscopy. Also, the ability to color the anodic layer was lower for low frequency pulse anodized surfaces. Komisarov et al.[25] have studied the structure of pulse anodized AA6063 and AA7075 alloys and observed variations in the pore morphology. Extensive pore branching in the anodic layer was observed for AA7075 compared to AA6063. Also, the regions of oxide growth under high current regime and low current regime could be differentiated when the difference between the high and low pulse amplitudes was high. However, for decorative applications, pulse anodizing and AC anodizing are traditionally not recommended due to the danger of deposition of sulfur and sulfur compounds in the anodic pores during the cathodic reaction and subsequent yellowness of the anodic layer.[26,27] Nevertheless, with addition of heavy metals during anodizing, the colors that can be imparted to the AC anodized surfaces showed very good light fastness.[28–30] Balasubramanian et al.[31] have studied the effect of Na_2SO_4 additive to sulfuric acid electrolyte for decorative AC anodizing and particularly on the deposition of sulfur into the anodic matrix. Results showed that the alloys which cannot be easily anodized under DC conditions can be anodized effectively under AC conditions.

Based on the above investigations, the present work focuses on investigating the high frequency pulse and pulse reverse pulse technique for anodizing the Al-TiO_2 surface composites. The effect of high frequency anodizing using a zero (pulse technique) or negative (pulse reverse pulse) potential during cathodic cycle (low voltage cycle) is investigated on the resulting microstructure and optical appearance of the anodized surface. Transmission electron microscopy (TEM) was employed for observing the cross sections prepared using focused ion beam scanning electron microscope (FIB-SEM) in situ lift-out technique. Various microstructural and morphological features of the anodized layer are presented and the underlying mechanism during anodizing is discussed.

Experimental

Surface composite preparation.— Aluminium substrates of dimensions 200 mm × 60 mm × 6 mm (Peraluman 853, Alcan rolled products, Germany) were obtained in the rolled condition. Commercial powders of TiO_2 (D_{50} = 210 nm, Ti Pure R900, DuPont Titanium Technologies, Belgium) were used for preparing the surface composites. Friction stir processing was performed to generate Al-TiO_2 surface composites. The experimental details of the process are described elsewhere.[9] The processed composite surfaces were mechanically polished to a mirror finish and subsequently degreased in a mild

[z]E-mail: vichg@mek.dtu.dk; chakri_gvc@yahoo.co.in

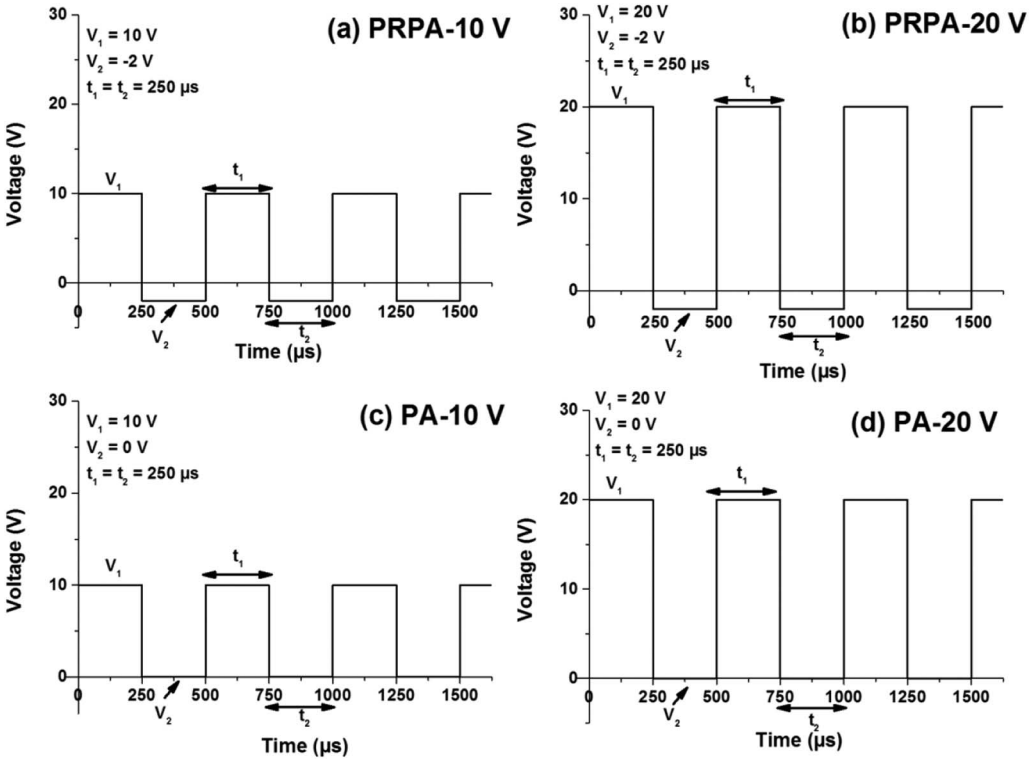

Figure 1. Voltage profiles used for high frequency Pulse Reverse Pulse Anodizing (a) PRPA-10 V, (b) PRPA-20 V; and Pulse anodizing (c) PA-10 V, (d) PA-20 V.

alkaline solution. Desmutting was performed by immersing in dilute HNO_3 followed by demineralised water rinsing. Finally the samples were ultrasonically cleaned in acetone for 15 min and dried in warm air.

High frequency anodizing.— The polished surface composites were then anodized in a 20 wt% sulfuric acid bath maintained at 10°C. Anodizing was performed by applying square voltage pulses (see Figure 1) from a function generator (33120A, Agilent Technologies). Waveforms of the voltage and current during the anodizing were monitored with the help of a digital oscilloscope (TDS3034B, Tektronix). The anodized area was approx. 2 cm^2. The potential during anodic cycle (V_1, high voltage cycle) was either 10 V or 20 V and during cathodic cycle (V_2, low voltage cycle) was either −2 V (pulse reverse pulse, called PRPA) or 0 V (pulse, called PA). The pulse frequency was fixed at 2 kHz and the duty cycle (i.e. the ratio between the anodic cycle duration and the time interval between two subsequent pulses) was fixed at 50% (i.e. $t_1 = t_2 = 250$ µs). The total anodizing time was adjusted for each sample so as to achieve an anodic layer thickness of approx. 10 µm.

Microstructural characterization.— The microstructure and morphology of the Al-TiO_2 composites and the obtained anodic layers were studied by a scanning electron microscope (Quanta 200 ESEM FEG, FEI) equipped with a back scatter electron detector (BSED) and energy dispersive spectroscopy (EDS) capability (80 mm^2 X-Max Silicon drift detector, Oxford Instruments). The SEM was typically operated at an acceleration voltage of 10 keV. For cross-sectional imaging, the samples were mounted in an epoxy and polished in cross-section. In order to minimize charging, the samples were coated by 2–3 nm Au layer by magnetron sputtering (Cressington 208 HR sputter coater). Transmission electron microscopy (TEM) analysis was carried out on the FSP and anodized sample cross section using a TEM (Model Tecnai G2 20) operating at 200 keV. The lamella for TEM were prepared using FIB-SEM in situ lift-out (Model Quanta 200 3D DualBeam, FEI) and further thinned for electron transparency in a FIB-SEM (Helios Nanolab DualBeam, FEI).

Results

Visual appearance of anodized surface.— The visual appearance of the anodized surfaces using different anodizing parameters is shown in Figure 2. The samples anodized using PRPA appear slightly brighter than the specimens anodized using PA irrespective of the potential during the anodic cycle. However, there is no significant difference in the brightness of the surfaces anodized with different anodic pulse amplitude. The striations observed in the anodized FSP Al-TiO_2 region are due to the forward movement of the FSP tool. The non-homogeneities in the distribution of the TiO_2 particles after FSP get revealed visually as striations after anodizing.

Microstructure of Al-TiO_2 surface composites.— Bright field TEM images of the FSP Al-TiO_2 composite, in cross section are shown in Figure 3a and 3b. It can be seen that the TiO_2 particles have not

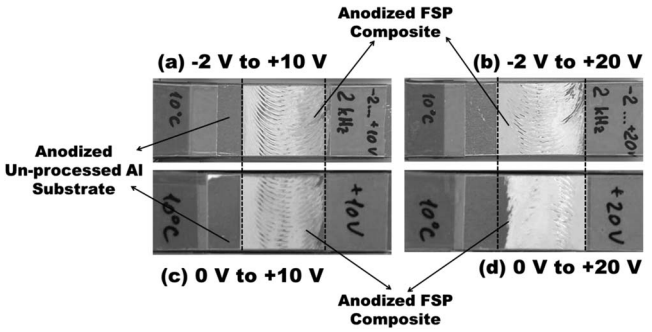

Figure 2. Optical images of anodized FSP Al-TiO_2 samples using: (a) PRPA-10 V (b) PRPA-20 V (c) PA-10 V and (d) PA-20 V.

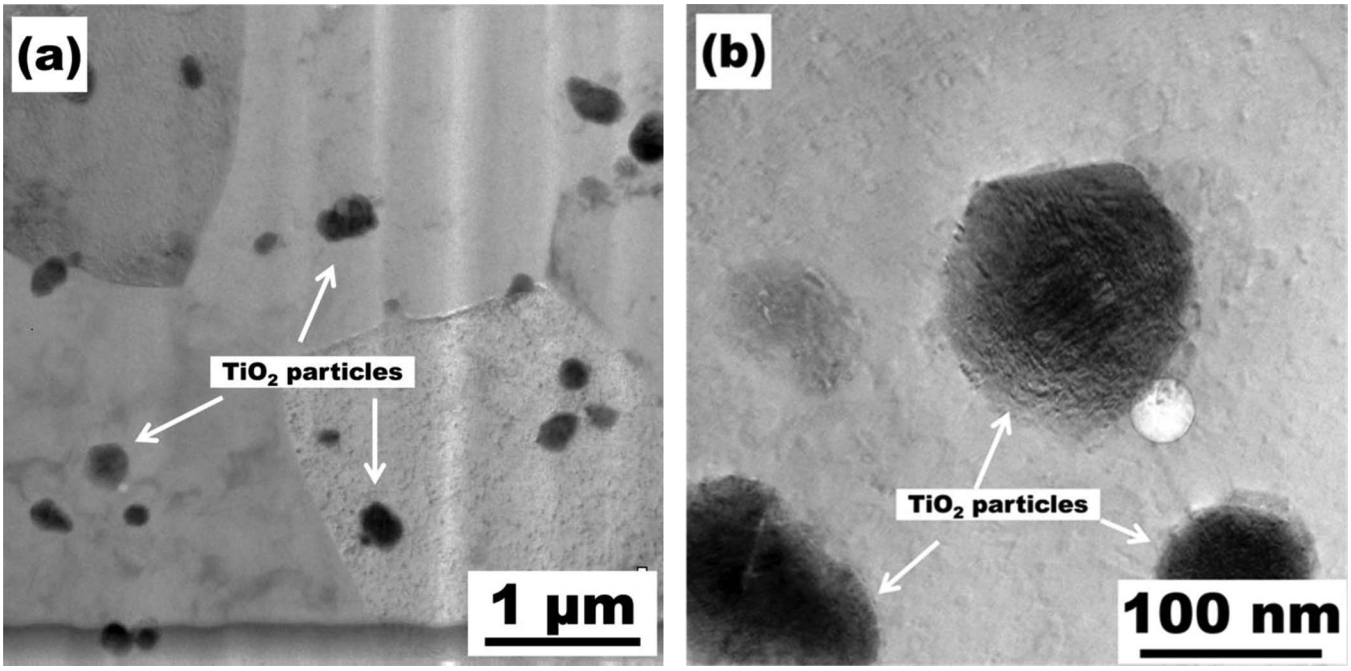

Figure 3. Bright field TEM cross section images of: (a) FSP Al-TiO_2 surface composites and (b) incorporated TiO_2 particle into the Al matrix, the circular hole at the edge of the particle is due to e-beam damage.

disintegrated during the FSP process and retained their spherical shape. The average size of the TiO_2 particles is approx. 200 nm. The particles are homogenously distributed in the Al matrix, and are found both within the grains and at the grain boundaries of the Al matrix. Further, there is no observable evidence of any porosity or voids near the TiO_2-Al matrix interface. There is no visible contrast at the interface hinting that there is very little reaction products at the interface due to chemical interactions between Al-TiO_2 during FSP (Figure 3b).

Microstructure of the anodized layer.–Scanning Electron Microscopy.— Figure 4a shows the cross-sectional image of the anodized layer after PRPA-10 V. The image shows dark spots on upper part of the anodized layer, while bottom part of the layer shows bright spots. The thickness of the anodized layer was approx. 10 µm.

It is observed that an increase in the anodic cycle potential to +20 V (PRPA-20 V) results in the appearance of these dark spots throughout the thickness of the anodic layer (see Figure 4b). EDS analysis (not shown here) of the bright and dark spots reveals the presence of Ti and O, suggesting that it corresponds to the TiO_2 particles incorporated in the anodized layer. However, for PA-10 V (see Figure 4c), the TiO_2 particles are present mostly as bright spots and increase of anodic cycle potential to +20 V (PA-20 V) caused more dark spots (see Figure 4d).

Transmission electron microscopy.–High Frequency Pulse Reverse Pulse Anodizing.— TEM bright field image of PRPA-10 V anodic layer in cross-section is shown in the Figure 5a. It can be seen that the bright as well as dark spots that were observed in the SEM-BSE cross-section image (Figure 4a) are TiO_2 particles in the anodic layer that are different in their morphology. The dark spots in the SEM-BSE image (Figure 4a) at the top half of the anodic layer correspond to TiO_2 particles in Figure 5a which are transformed to a porous morphology in the anodic matrix during anodizing or in some cases are completely lost leaving behind a void. The brighter spots observed in the SEM-BSE image at the bottom of the anodic layer correspond to denser TiO_2 particles, which are transformed to a lesser extent or are preserved in their crystalline state. Higher magnification image shows that the anodizing pores originate preferentially from the bottom of the TiO_2 particles (marked as pore branching), whereas in the surrounding matrix they appear continuous (Figure 5b). Further, the anodic layer-substrate interface has grown more inward into the substrate compared to the surrounding areas (Figure 5a). Similar morphological features are also observed for samples anodized using PRPA-20 V at 2 kHz as seen in Figure 6a and 6b.

High frequency pulse anodizing.— Figure 7 shows the bright field TEM images of the sample anodized using PA-10 V in cross section. The TiO_2 particles are intact in the anodic Al matrix and there is little observable transformation to porous morphology of the TiO_2 particles. These particles are observed as bright spots in the SEM-BSE image in Figure 4c. Voids on the top of the TiO_2 particles are seen in the anodic matrix. The anodized pore structure in this case is different from the structure observed for pulse reverse pulse anodizing technique (Figure 5 and Figure 6). The anodized pores appear to be growing around the TiO_2 particle unlike originating below the particle as in the case of PRPA-10 V and PRPA-20 V. Further, a clear discontinuity is observed in the anodic pore structure. Careful observation of the pore structure shows that the anodizing process has not completely progressed under the TiO_2 particles (marked as incomplete anodizing in Figure 7a, and 7b). The bright field TEM images of sample anodized with PA-20 V at 2 kHz in cross section is shown in Figure 8. The effect of increasing the anodic cycle voltage can be clearly observed in terms of the progress of the pores under the TiO_2 particles. The TiO_2 particles are completely surrounded by pores unlike the features observed in Figure 7 but are not originating from the TiO_2 particle-anodic matrix interface like seen in Figure 5 and Figure 6. The anodic pore structure observed is intermittent and discontinuous similar to that observed for the PA-10 V sample.

Discussion

Friction stir processing of Al with TiO_2 provided surface composites with little or no degradation of the TiO_2 particles. There are no observable voids or discontinuities between the TiO_2 particles and the Al matrix, and no bulk reaction products are observed (see Figure 3). The temperature involved during FSP of Al is reported to be between 400–450°C.[32] Although the increase in temperature during the FSP process is enough for the formation of Al-Ti intermetallic phases,[33–35]

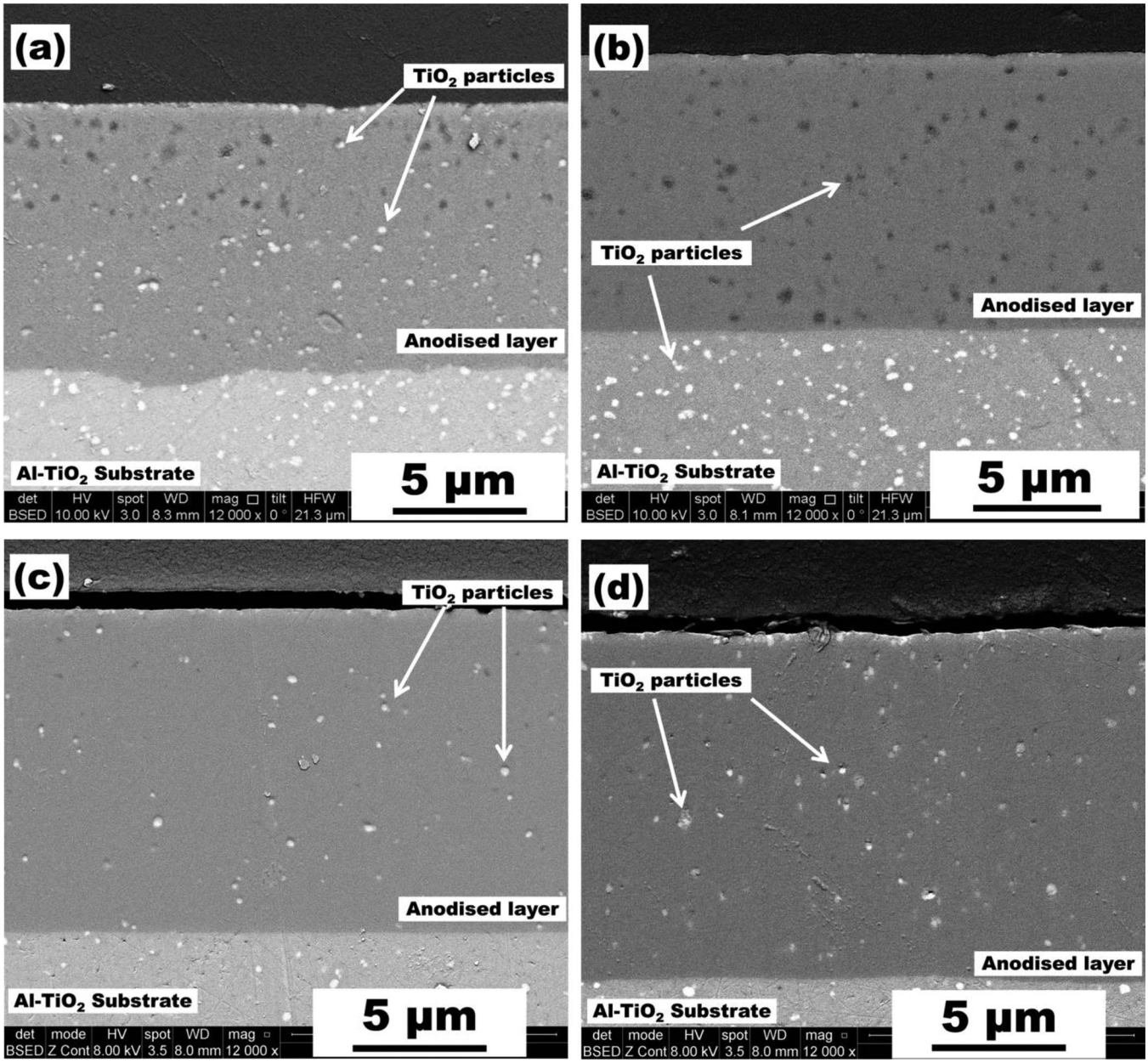

Figure 4. SEM-BSE cross-section image of the FSP Al-TiO_2 sample anodized using: (a) PRPA-10 V, (b) PRPA-20 V, (c) PA-10 V, and (d) PA-20 V at 2 kHz. (The TiO_2 particles can be seen in the Al-TiO_2 composite substrate and also in the anodized layer as both bright and dark spots.)

the quenching effect provided by high cooling rate of the thick Al base plate might have reduced the reaction kinetics. Gudla et al.,[9] using grazing incidence X-ray diffraction, showed that the FSP process itself does not cause any considerable formation of Al-Ti based phases under the same processing conditions.

Anodizing using pulse reverse pulse technique (PRPA) shows visually brighter surfaces when compared to pulse anodizing (PA) (see Figure 2). The microstructure of the anodic layer obtained using PRPA shows transformation to porous morphology and subsequent loss of TiO_2 particles in the anodized layer and the effect is increased with increase in the anodic cycle potential (Figure 4a and 4b). However, when only PA is used, the TiO_2 particles are incorporated and retained in the anodic layer to a higher extent (Figure 7 and Figure 8) both in transformed and non-transformed states. The other main difference in the morphology of the anodic layer is that of the observed anodic pore structure. The PRPA technique shows pores originating from the bottom of the TiO_2 particles (Figure 5 and Figure 6) whereas the anodic pores are observed to be growing around the TiO_2 particles under PA conditions (Figure 7 and Figure 8). Also, the completeness of the anodizing beneath the particles is observed to be higher for PA-20 V when compared to PA-10 V.

Gudla et al.,[9] using grazing incidence X-ray diffraction, have reported the existence of various kinds of Ti-O phases of general formula Ti_nO_{2n-1} (magneli phases) in the anodized layer of Al-TiO_2 surface composites after being subjected to conventional DC sulfuric acid anodizing. This generation of oxygen defects in the TiO_2 was attributed to the combined effect of sulfuric acid electrolyte and the applied anodizing potential. The presence of magneli phases[36] increases the electrical conductivity of the TiO_2.[37,38] The electrical properties of the Ti-O phases under AC conditions are frequency and temperature dependent as shown by Regonini et al.[39] The conductivity of the phases is observed to be six orders of magnitude higher than TiO_2 (rutile) at room temperature measured at 2 kHz AC frequency.[40] This increased conductivity makes the Ti-O magneli phases in the anodic

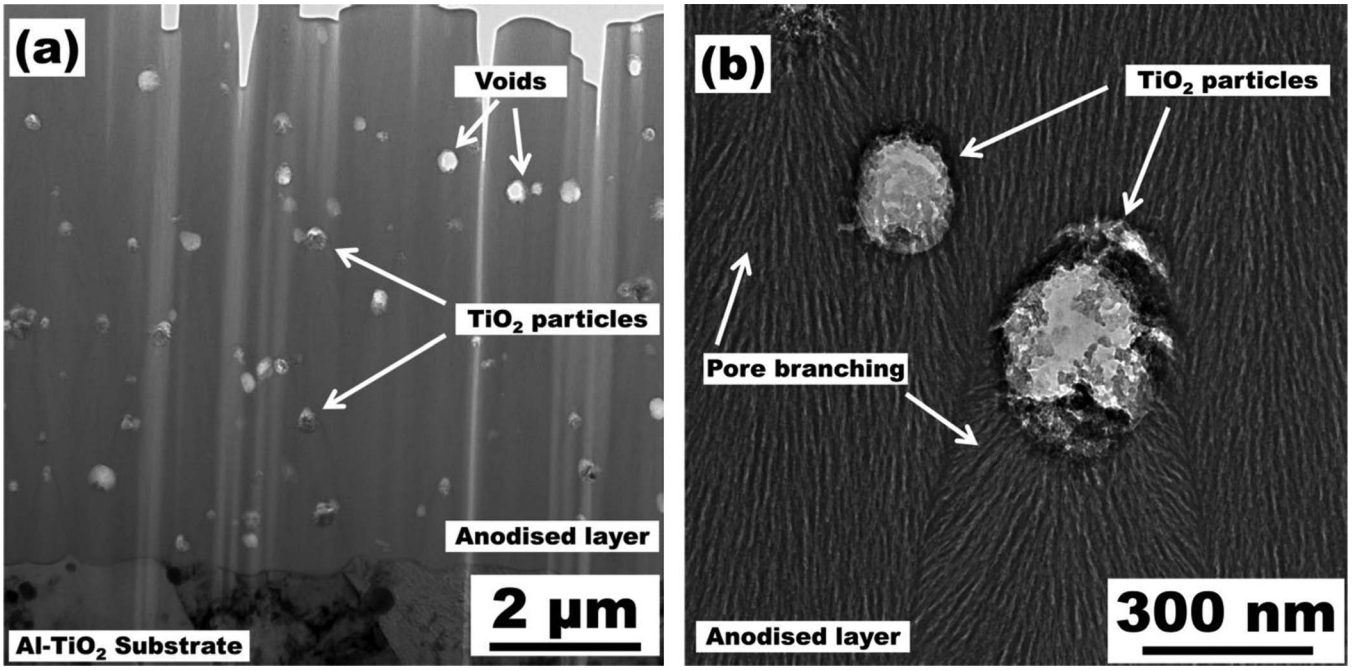

Figure 5. Bright field TEM cross-section images of FSP Al-TiO_2 sample anodized using (a) PRPA-10 V at 2 kHz showing (b) transformed TiO_2 particles in the anodic matrix and preferential origin of anodic pores from the TiO_2 particle-Al interface.

layer more conductive under AC/pulse conditions at high frequency compared to the conventional DC anodizing.

The observed morphology and structure of the anodized layer for high frequency PRPA and PA of Al-TiO_2 composites is schematically shown in Figure 9 as sequence of possible steps. Under PRPA, anodic oxidation of Al and consequent film growth takes place under the applied positive potential (+10 V or +20 V). The film grows uniformly over the particle free Al matrix and in the surrounding areas of the TiO_2 particles, which are at the anodic oxide-substrate interface. The TiO_2 particles are assumed to remain chemically inert during the anodic or positive cycle. At the end of positive cycle, the TiO_2 particles are partially surrounded by the anodic Al-oxide that is formed (Figure 9b). The possibility of formation of a barrier type anodic alumina layer over the TiO_2 particles is not clear yet. During the cathodic or negative cycle of PRPA, the anodic film on Al ceases to grow and cathodic reactions like hydrogen gas evolution (and cathodic deposition of elements such as Sulfur) take place[41] if there is sufficient negative potential applied to allow for current through the barrier layer. In the

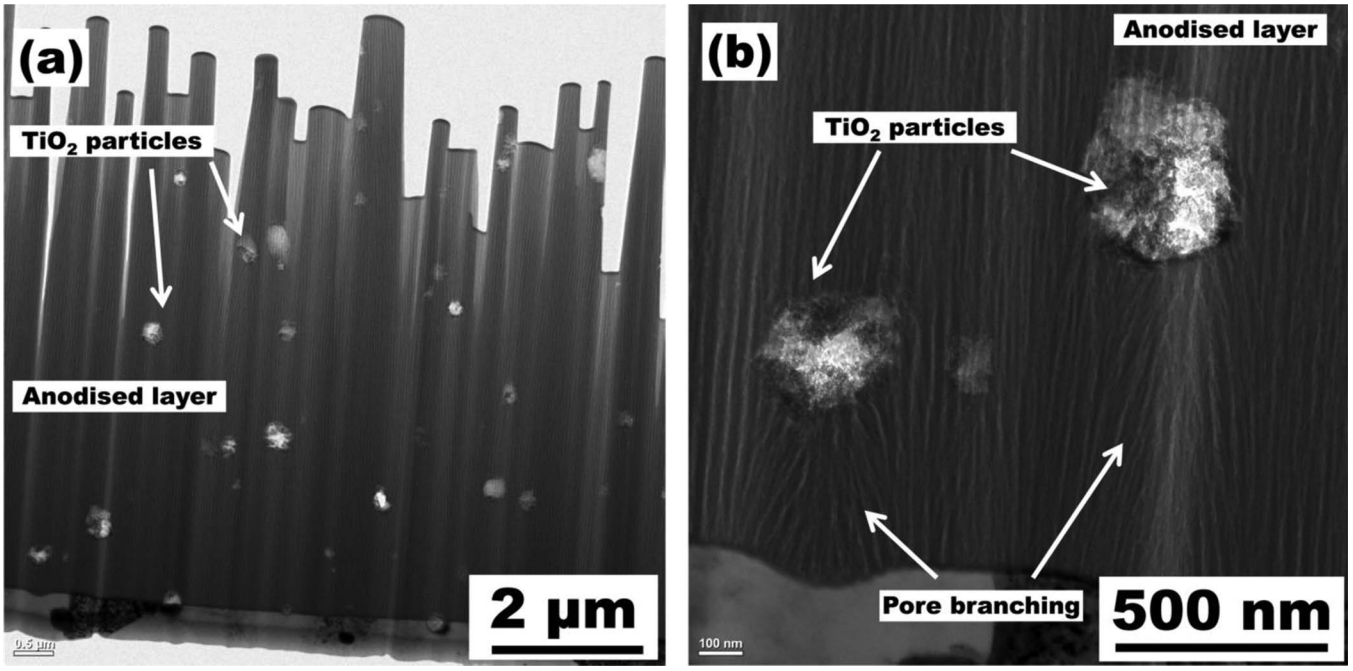

Figure 6. Bright field TEM cross-section image of FSP Al-TiO_2 sample anodized using (a) PRPA-20 V at 2 kHz showing (b) transformed TiO_2 particles in the anodic matrix and preferential origin of anodic pores from the TiO_2 particle-Al interface.

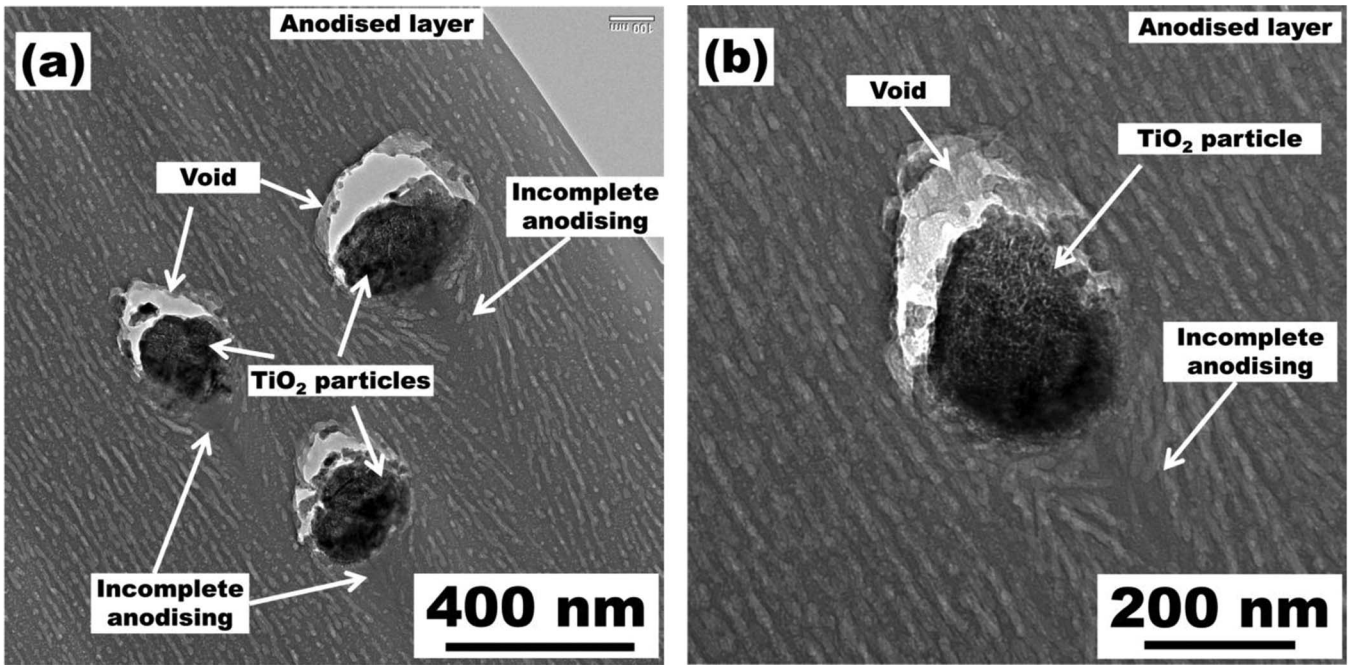

Figure 7. Bright field TEM cross-section image of FSP Al-TiO_2 sample anodized using (a) PA-10 V at 2 kHz showing (b) TiO_2 particles with voids on the top that are incorporated into the anodic layer and incomplete progress of anodic pores below the particles.

present situation, the applied negative cycle is only −2 V and is not sufficient for current flow through the barrier layer. However, as the TiO_2 (containing magneli phases) is more electrically conducting than the barrier anodic Al oxide, the cathodic current gets localized (due to lower electrical resistance) at the particles that are partially in the substrate Al metal matrix and partially surrounded by the anodic Al oxide. As a result, the cathodic reactions like hydrogen gas evolution take place more vigorously at the TiO_2 particle-electrolyte interface when compared to that at the barrier layer-electrolyte interface (Figure 9c). This localized vigorous gas evolution causes the barrier anodic Al oxide (if formed during the previous anodic cycle) over the TiO_2 particles and the surrounding porous anodized alumina to get mechanically weakened or completely disintegrated generating porosity and voids at the TiO_2 particle-anodized layer interface. Other factors that might contribute to porosity at the interface are the formation of oxygen during the anodic oxidation[42–45] and density mismatch between the growing anodized oxide and the TiO_2 particle. However, hydrogen evolution during cathodic cycle is very vigorous, therefore expected to be a greater contributing factor. As a result of this porosity, the electrical resistance at the interface of the TiO_2 particles-anodized

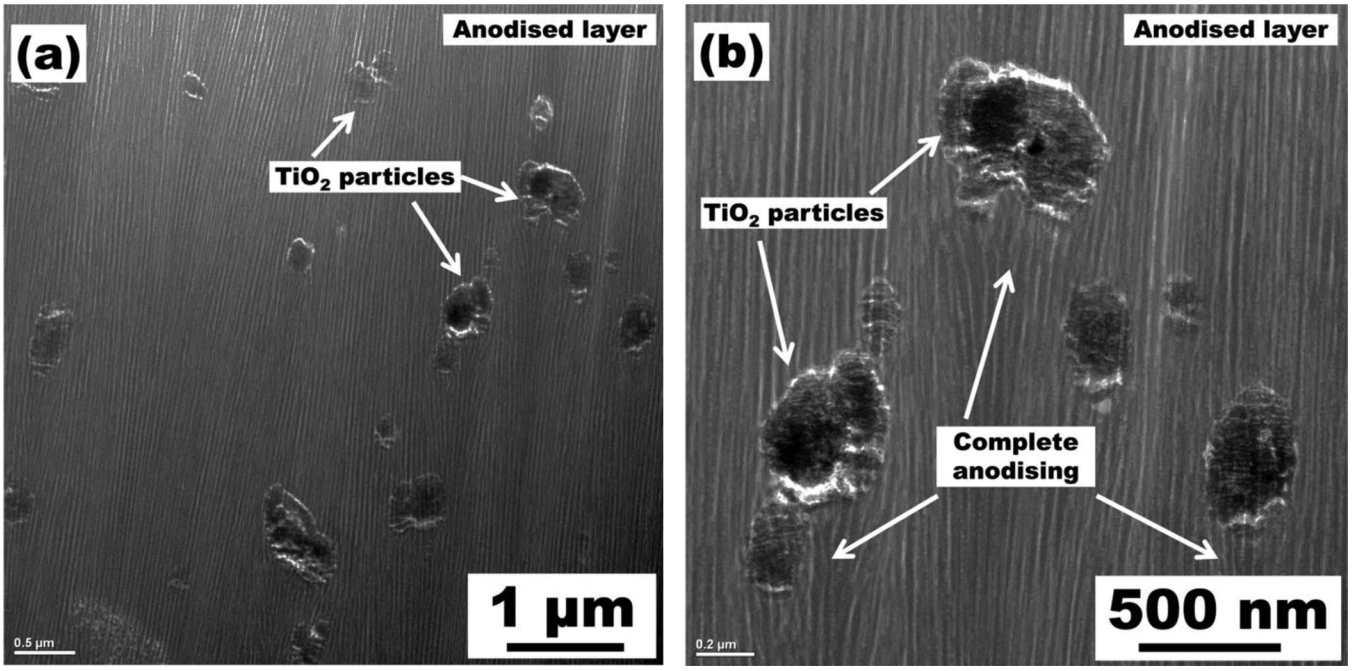

Figure 8. Bright field TEM cross-section image of FSP Al-TiO_2 sample anodized using (a) PA-20 V at 2 kHz showing (b) TiO_2 particles that are incorporated into the anodic layer and coverage of anodic pores below the particles.

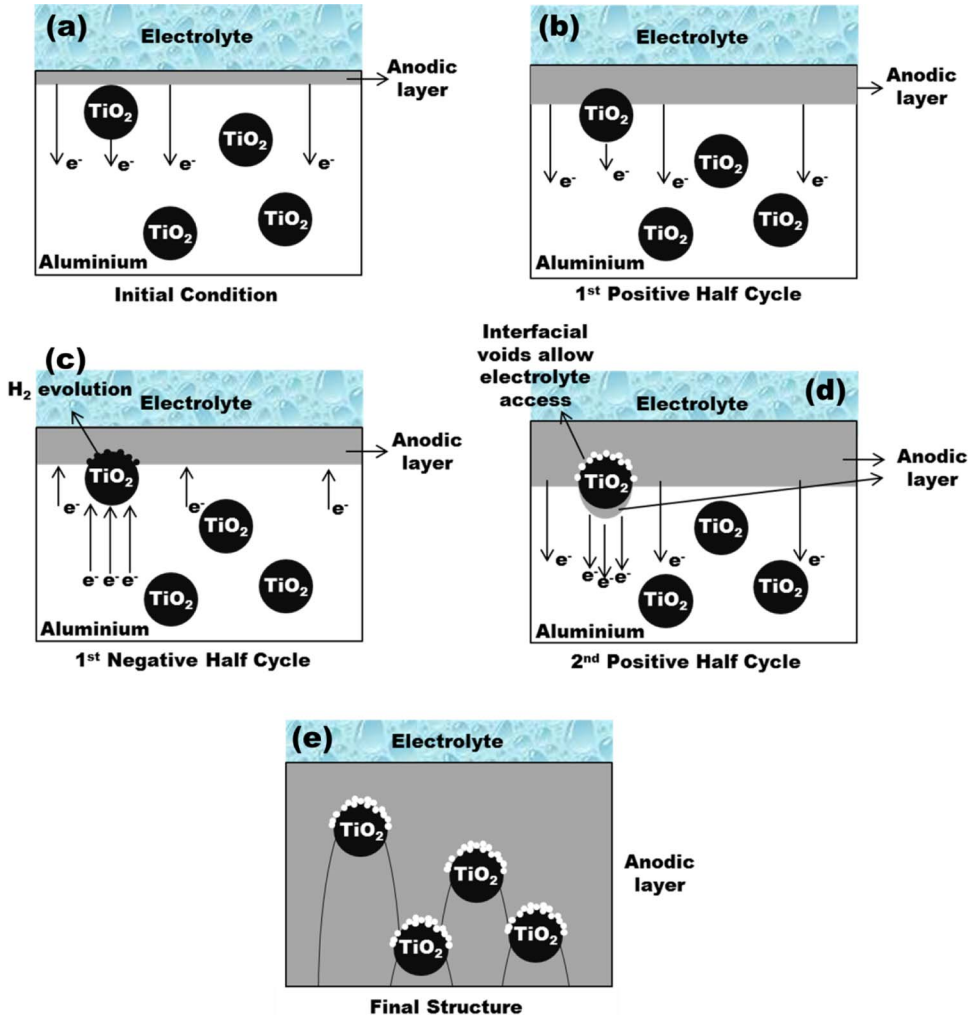

Figure 9. Schematic showing the (a) to (e) stepwise anodic film growth on Al-TiO_2 composite and successive incorporation of TiO_2 particles during high frequency pulse reverse pulse anodizing (PRPA).

layer-Al substrate junctions is further reduced.[46] In parallel, during the cathodic cycle, the anodized barrier layer on the particle free interface is also expected to be reduced in thickness due to chemical dissolution by the anodizing electrolyte. But, in the present scenario the cathodic cycle time is only 250 μs and according to the dissolution rates reported by Zhang et al.[47] for anodized barrier oxides in sulfuric acid thinning of barrier layer can be neglected.

During the next positive or anodic cycle, the anodic film growth takes place evenly on the particle free Al areas (Figure 9d). Since the TiO_2 is conducting and also the electrical resistance is lowered at the particle locations due to hydrogen evolution and subsequent mechanical weakening of the anodic oxide, the anodic current is localized to a higher extent at the TiO_2 particle-substrate interface. The generated porosity or voids in the cathodic cycle at the TiO_2 particle-Al matrix allows easy access for the anodizing electrolyte and porous anodic film growth begins at the interface. This result of this phenomenon can be observed in Figure 5 and Figure 6, where the anodizing pores are originating from the TiO_2 particle-matrix interface. This localization of anodic current at the TiO_2 particles results in a faster anodized film growth beneath the particles and leads to the anodic structure as observed in Figure 9e.

Under high frequency pulse anodizing conditions (PA), the applied potential during the cathodic cycle is only 0 V and hence the corresponding cathodic reactions will not take place. When the second cycle of anodic potential is impressed upon the system, the anodic film continues to grow more or less at the same rate in particle free areas and also around the particles. Once the TiO_2 particles are embedded into the oxide, they lose electrical contact from the substrate matrix and hence the anodized layer does not show any pores generated at the TiO_2 particle-anodized matrix interface (Figure 7 and Figure 8). The extent of coverage of the TiO_2 particles by the anodized alumina matrix is observed to be dependent on the amplitude of the anodic cycle potential that is applied (+10 V or +20 V). The higher the potential applied, better the anodic pores surrounding the TiO_2 particle (Figure 8). Gudla et. al[7–9] have shown with the use of sputter deposited Al-Zr coatings that un-anodized metallic phases and left over aluminum matrix in an anodic layer contribute to darkening of the anodic layer. This phenomenon may be one of the reasons behind the slightly darker appearance of pulse anodized (PA) surfaces when compared to pulse reverse pulse anodized (PRPA) surfaces (see Figure 2) as there is more probability of presence of un-anodized Al under the TiO_2 particles for PA technique (especially PA-10 V).

In Figure 5 there are locations where the TiO_2 particles are lost from the anodic matrix leaving behind voids. This is assumed to be due to the vigorous hydrogen gas evolution during the cathodic cycle. Factors like reduction in mechanical integrity of the interface and volume expansion as well as dissolution of the surrounding Al oxide combine to expulse the TiO_2 particles.

Conclusions

High frequency pulse reverse pulse (PRPA) and pulse anodizing (PA) of friction stir processed Al-TiO_2 surface composites showed that the potential applied during the cathodic cycle has significant effect on the resulting anodic pore structure. Pulse reverse pulse anodizing caused anodic pores to nucleate and grow under the TiO_2 particles and at the particle-Al matrix interface due to cathodic current localization caused by combined effect of increased electrical conductivity of TiO_2 and mechanical weakening of anodic oxide at particle-oxide interface. High frequency pulse anodizing resulted in the anodic pores to grow normally and uniformly around the TiO_2 particles. Increase in anodic cycle potential does not affect the structure of the anodic layer considerably in case of pulse reverse pulse anodizing (PRPA), but for pulse anodizing (PA) the uniformity of coverage of TiO_2 particles with anodic pores is improved.

Acknowledgments

The authors thank all the involved ODAAS project partners. The financial funding from the Danish National Advanced Technology Foundation for the ODAAS project is greatly acknowledged. Aude Simar acknowledges the financial support from the Interuniversity Attraction Poles Program from the Belgian State through the Belgian Policy agency; contract IAP7/21 "INTEMATE".

References

1. P. G. Sheasby and R. Pinner, *The Surface Treatment and Finishing of Aluminium and Its Alloys*, Volume 1, 6th ed., p. 1, ASM International; Finishing Publications, (2001).
2. P. G. Sheasby and R. Pinner, *The Surface Treatment and Finishing of Aluminium and Its Alloys*, Volume 2, 6th ed., p. 1, ASM International; Finishing Publications, (2001).
3. C. A. Grubbs, *Met. Finish.*, **105**, 397 (2007).
4. C. A. Grubbs, *Met. Finish.*, **93**, 449 (1995).
5. G. E. Thompson and G. C. Wood, *Nature*, **290**, 230 (1981).
6. M. Aggerbeck, A. Junker-Holst, D. V. Nielsen, V. C. Gudla, and R. Ambat, *Surf. Coatings Technol.*, **254**, 138 (2014).
7. V. C. Gudla, S. Canulescu, R. Shabadi, K. Rechendorff, J. Schou, and R. Ambat, in *Light Metals 2014*, J. Grandfield and J. TMS, Editors, vol. **317**, p. 369, John Wiley & Sons, Inc. (2014).
8. V. C. Gudla, S. Canulescu, R. Shabadi, K. Rechendorff, K. Dirscherl, and R. Ambat, *Appl. Surf. Sci.*, **317**, 1113 (2014).
9. V. C. Gudla, F. Jensen, A. Simar, R. Shabadi, and R. Ambat, *Appl. Surf. Sci.*, **324**, 554 (2015).
10. K. Shimizu, G. M. Brown, K. Kobayashi, P. Skeldon, G. E. Thompson, and G. C. Wood, *Corros. Sci.*, **40**, 1049 (1998).
11. M. Jariyaboon, P. Møller, R. E. Dunin-Borkowski, and R. Ambat, *Anti-Corrosion Methods Mater.*, **58**, 173 (2011).
12. J. C. Walmsley, C. J. Simensen, A. Bjørgum, F. Lapique, and K. Redford, *J. Adhes.*, **84**, 543 (2008).
13. M. Saito, *J. Electrochem. Soc.*, **140**, 1907 (1993).
14. J. Timm, *Key Eng. Mater.*, **44–45**, 219 (1990).
15. A. E. Hultquist, *J. Electrochem. Soc.*, **111**, 1302 (1964).
16. R. Chang and W. F. Hall, *Thin Solid Films*, **46**, L5 (1977).
17. T. Yamamoto, H. Tanaka, M. Fujita, H. Asoh, and S. Ono, *J. Japan Inst. Light Met.*, **60**, 602 (2010).
18. D. Kanagaraj, V. Raj, S. Vincent, and S. V. Iyer, *Bull. Electrochem.*, **17**, 523 (2001).
19. D. Kanagaraj, V. Raj, S. Vincent, B. P. Kumar, A. S. Kumar, and S. V. Iyer, *Bull. Electrochem.*, **17**, 285 (2001).
20. A. Deacon *Juhl, Thesis, Technical University of Denmark* (1999).
21. K. Yokoyama, H. Konno, H. Takahashi, and M. Nagayama, *Plat. Surf. Finish.*, **69**, 62 (1982).
22. C. Colombini, *Finishing*, **12**, 34 (1988).
23. K. Okubo, S. Toba, and Y. Sakura, *J. Met. Finish. Soc. Japan*, **39**, 512 (1988).
24. K. Okubo, S. Suyama, and Y. Sakura, *J. Surf. Finish. Soc. Japan*, **40**, 1366 (1989).
25. V. Komisarov and A. R. Thölén, *Mater. Sci. Eng. A*, **151**, 197 (1992).
26. I. De Graeve, H. Terryn, and G. E. Thompson, *Electrochim. Acta*, **52**, 1127 (2006).
27. J. M. Kape, *Met Finish J*, **20**, 80 (1974).
28. J. M. Kape, *Trans. Inst. Met. Finish.*, **55**, 25 (1977).
29. J. M. Kape, *Trans. Inst. Met. Finish.*, **66**, 41 (1988).
30. J. M. Kape, *Trans. Inst. Met. Finish.*, **63**, 90 (1985).
31. V. Balasubramanian, S. John, and B. A. Shenoi, *Surf. Technol.*, **19**, 293 (1983).
32. R. S. Mishra, Z. Y. Ma, and I. Charit, *Mater. Sci. Eng. A*, **341**, 307 (2003).
33. Q. Zhang, B. L. Xiao, D. Wang, and Z. Y. Ma, *Mater. Chem. Phys.*, **130**, 1109 (2011).
34. Q. Zhang, B. L. Xiao, Q. Z. Wang, and Z. Y. Ma, *Mater. Lett.*, **65**, 2070 (2011).
35. C. J. Hsu, C. Y. Chang, P. W. Kao, N. J. Ho, and C. P. Chang, *Acta Mater.*, **54**, 5241 (2006).
36. G. V Samsonov, *The Oxide Handbook*, IFI/Plenum, London, (1973).
37. M. Li, W. Hebenstreit, U. Diebold, A. M. Tyryshkin, M. K. Bowman, G. G. Dunham, and M. A. Henderson, *J. Phys. Chem. B*, **104**, 4944 (2000).
38. U. Diebold, *Surf. Sci. Rep.*, **48**, 53 (2003).
39. D. Regonini, A. C. E. Dent, C. R. Bowen, S. R. Pennock, and J. Taylor, *Mater. Lett.*, **65**, 3590 (2011).
40. D. Regonini, V. Adamaki, C. R. Bowen, S. R. Pennock, J. Taylor, and A. C. E. Dent, *Solid State Ionics*, **229**, 38 (2012).
41. G. E. Thompson, R. C. Furneaux, and G. C. Wood, *Corros. Sci.*, **18**, 481 (1978).
42. L. Kompotiatis and I. Kaplanoglou, *Corosion Sci.*, **40**, 1939 (1998).
43. M. Saenz De Miera, M. Curioni, P. Skeldon, and G. E. Thompson, *Surf. Interface Anal.*, **42**, 241 (2010).
44. X. Zhu, L. Liu, Y. Song, H. Jia, H. Yu, X. Xiao, and X. Yang, *Mater. Lett.*, **62**, 4038 (2008).
45. X. F. Zhu, D. D. Li, Y. Song, and Y. H. Xiao, *Mater. Lett.*, **59**, 3160 (2005).
46. J. Zahavi, *J. Electrochem. Soc.*, **129**, 1572 (1982).
47. L. Zhang, G. E. Thompson, M. Curioni, and P. Skeldon, *J. Electrochem. Soc.*, **160**, C179 (2013).